Physica Medica 68 (2019) 146–154

Contents lists available at ScienceDirect

Physica Medica

journal homepage: www.elsevier.com/locate/ejmp

Technical note

Performance evaluation of a new time of flight PET/CT scanner: Results of a multicenter study

Alessandra Zorz[a,*,1], Roberta Matheoud[b,1], Elisa Richetta[c], Saraswati Baichoo[d,e], Matteo Poli[c], Alessandro Scaggion[a], Riccardo Emanuele Pellerito[f], Lea Cuppari[g], Gian Mauro Sacchetti[h], Michele Stasi[c], Marta Paiusco[a], Marco Brambilla[b]

[a] Medical Physics Department, Veneto Institute of Oncology IOV – IRCCS, via Gattamelata 64, Padua, Italy
[b] Medical Physics Department, AOU Maggiore della Carità, Corso Mazzini 18, Novara, Italy
[c] Medical Physics Department, AO Ordine Mauriziano di Torino, Via Magellano 1, Turin, Italy
[d] Dept. of Physics, University of Trieste, Via Tiepolo 11, Trieste, Italy
[e] Abdus Salam International Centre for Theoretical Physic (ICTP), Strada Costiera 11, Trieste, Italy
[f] Nuclear Medicine Department, AO Ordine Mauriziano di Torino, Via Magellano 1, Turin, Italy
[g] Nuclear Medicine Department, Veneto Institute of Oncology IOV – IRCCS, via Gattamelata 64, Padua, Italy
[h] Nuclear Medicine Department, AOU Maggiore della Carità, Corso Mazzini 18, Novara, Italy

ARTICLE INFO

Keywords:
Positron Emission Tomography
Performance
Image quality

ABSTRACT

Purpose: The aim of this multicenter study was to evaluate the performance of the upgraded version of the Ingenuity TF PET/CT scanner, according to the NEMA NU-2 2012 standards.

Methods: Spatial resolution, sensitivity, count rate response, scatter fraction, image quality and accuracy were evaluated on three Ingenuity TF scanners installed in Italian hospitals. Furthermore, energy and timing resolution were measured. A detailed image quality phantom analysis was performed to evaluate the effect of different clinical reconstruction parameters, including the application of PSF correction.

Results: Results show an average spatial resolution of 4.7 mm and an average absolute system sensitivity of 7.9 cps/kBq. The average maximum NECR was 119.83 kcps at 20.67 kBq/ml, while the maximum true event rate was 322.62 kcps at the concentration of 24.51 kBq/ml. The average maximum bias below NECR peak was 12.58%. All the results of NEMA tests were in agreement with the values declared by the manufacturer. The estimated average energy and timing resolution were 10.83% and 536.2 ps, respectively.

Image quality phantom analysis obtained with different reconstruction settings showed that PSF correction was the parameter that affected mainly on contrast recovery coefficient, while the iteration number and amplitude of Gaussian filter had no significant effect. Of relevance, the application of PSF correction never led to recovery coefficient values higher than 100% and to Gibbs or edge artifacts.

Conclusions: The new Ingenuity TF model shows physical performance similar to other scanners of the latest generation for all standard NEMA NU2-2012 measurements.

1. Introduction

The Philips Ingenuity TF 64 PET/CT (Philips Healthcare, Cleveland, OH, USA) is a new hybrid scanner (2017) combining a time-of-flight (TOF) Positron Emission Tomography (PET)-capable with a 64-slice Computed Tomography (CT). The Ingenuity TF upgraded version is equipped with the new PIXELAR detector design with continuous light guide; additionally, this new model is compliant with the European council directive 2002/95/CE "Restriction of Hazardous Substances Directive" (RoHS), which involves a complete redesign of the electronic components with respect to the previous model. The fast timing properties, combined with this new design, lead to a high sensitivity scanner

* Corresponding author at: Medical Physics Department, Veneto Institute of Oncology IOV – IRCCS, Via Gattamelata n. 64, 35128 Padova, Italy.
E-mail addresses: alessandra.zorz@iov.veneto.it (A. Zorz), roberta.matheoud@maggioreosp.novara.it (R. Matheoud), erichetta@mauriziano.it (E. Richetta), saraswati.baichoo@gmail.com (S. Baichoo), mpoli@mauriziano.it (M. Poli), alessandro.scaggion@iov.veneto.it (A. Scaggion), repellerito@mauriziano.it (R.E. Pellerito), lea.cuppari@iov.veneto.it (L. Cuppari), gianmauro.sacchetti@maggioreosp.novara.it (G.M. Sacchetti), mstasi@mauriziano.it (M. Stasi), marta.paiusco@iov.veneto.it (M. Paiusco), marco.brambilla@maggioreosp.novara.it (M. Brambilla).
[1] Alessandra Zorz and Roberta Matheoud equally contributed to this work and should be considered as co-first authors.

https://doi.org/10.1016/j.ejmp.2019.11.017
Received 26 June 2019; Received in revised form 14 November 2019; Accepted 18 November 2019
Available online 28 November 2019

with good counting rate capability.

To our knowledge, no studies have reported the results of performance measurements according to National Electrical Manufacturers Association (NEMA) NU-2 2012 [1] on the new Ingenuity TF RoHS PET/CT scanner.

The aim of this multicenter study was to evaluate PET performances according to the 2012 version of the NEMA standards on three PET Ingenuity TF 64 scanners installed in Italian hospitals (1. Istituto Oncologico Veneto IOV-IRCCS, Padua; 2. Azienda Ospedaliero Universitaria Maggiore della Carità, Novara; 3. AO Ordine Mauriziano di Torino, Turin). In particular, spatial resolution, sensitivity, count rate response, scatter fraction, image quality and accuracy were evaluated. A comparison with the performance results obtained by Kolthammer et al. [2] with NEMA NU-2 2007 [3] standards on the previous Ingenuity TF model was performed. Moreover, as quantitative analysis in PET/CT imaging is becoming increasingly important in 18F-FDG oncological studies [4], it is fundamental to investigate the impact that different reconstruction parameters and advanced reconstruction modalities (resolution modelling) may have on the recovery coefficients and background variability. Therefore, additional phantom analyses were performed to evaluate these effects on image quality.

2. Materials and methods

A set of acceptance measurements were obtained on three different PET/CT Ingenuity TF scanners. PET performances were evaluated following the NEMA NU 2-2012 protocol [1]. Before each measurement, a daily quality control with a gain, energy and time calibration was performed.

2.1. Ingenuity TF scanner

The Ingenuity TF 64 PET/CT scanner (Philips Healthcare, Cleveland, OH, USA) is equipped with 28,336 lutetium – yttrium oxyorthosilicate (LYSO) detectors and TOF technology. The PET ring diameter is 90 cm with an axial Field of View (FOV) of 18 cm. The 28 modules are organized in 23 by 44 matrices of $4 \times 4 \times 22$ mm^3 LYSO crystal coupled to 420 hexagonal photomultiplier tubes with the PIXELAR detector design and a continuous light guide. Data are exclusively acquired in a three-dimensional (3D) list-mode format. The energy window is set between 440 and 665 keV. The available reconstruction transverse FOVs are 256, 576 and 676 mm, respectively for brain, standard whole-body and large patient acquisitions. The coincidence window is 3.8 ns for the 576 mm FOV, shorter than the 4.5 ns hardware coincidence window of the previous Ingenuity model [2].

The CT component is a 64 slice scanner with a 4 cm axial coverage.

Images are reconstructed using a TOF, list-mode, blob-based, ordered subsets maximum likelihood expectation maximization algorithm (TOF-OSEM) [5]. Attenuation, scatter, random, detector normalization, isotope decay, system dead time and crystal timing corrections are applied. Scatter is estimated through a combination of single scatter and Monte Carlo simulation. Random correction uses a smoothed delay-line random coincidence correction method. The TOF information is included as a TOF kernel width, which compensates for changes in time resolution as a function of measured detector count rate by setting the kernel width according to the average singles rate in each frame.

Three levels are available for the “Speed” parameter, namely Fast, Normal and High Quality, which correspond to 60, 99 and 99 iterations and a TOF kernel width of 14.1, 14.1 and 18.7 cm, respectively.

Four levels are available for the “Smooth/Sharp” parameter, namely Normal, Smooth, SmoothA and SmoothB, which correspond to the values of 1.0, 0.7, 0.6 and 0.5 for the relaxation parameter and to 4, 5, 6 and 7 mm for the amplitude of the Gaussian filter, respectively. The relaxation parameter is a factor used to weight each iteration; a relaxation parameter inferior than 1 means a less significant iteration update in the reconstruction process.

The user is not allowed to independently select the number of iterations and TOF kernel. Indeed, changing the “Speed” parameter means both a modification in number of iterations and TOF kernel width in a pre-defined set.

The manufacturer’s suggested reconstruction parameters for the standard body protocol are Normal “Speed” and Normal “Smooth/Sharp”, which correspond to the combination 3x33 equivalent iterations and a relaxation parameter equal to 1, with 4 mm for the amplitude of the Gaussian filter.

The reconstruction algorithm also allows for the option of Point-Spread Function recovery (PSF) with Richardson-Lucy maximum-likelihood resolution recovery methods, in which the number of recovery iterations and the Gaussian regularization kernel width specified in mm (FWHM) can be selected [6]. One or two iterations are sufficient to achieve good resolution recovery, while a regularization kernel similar to the system resolution is preferable. Manufacturer’s recommendations suggest one iteration and a 6 mm FWHM regularization kernel, in order to balance a good resolution recovery without excessive noise amplification.

The high-resolution reconstruction protocol, with 2 mm image voxel, is also available.

2.2. Energy resolution and timing resolution

The energy and the TOF resolution were measured with a 22Na point source of 3.7 MBq. The point source was positioned in the centre of the scanner FOV with a brass block (manufacturer source holder). Manufacturer’s protocol was used for the emission scan acquisition and analysis.

2.3. Sensitivity

The source consisted of a 70 cm polyethylene tube (internal diameter: 2 mm) filled with an average activity of 6.57 MBq (4.9–7.6 MBq) (the manufacturer’s suggested activity was 7 MBq) of 18F-fluorodeoxyglucose (FDG). The activity should be sufficiently low so that the percent dead time losses are less than 5% and the random coincidence rate is less than 5% of the total event rate. The tube was inserted into five concentric aluminium sleeves (NEMA PET Sensitivity Phantom, Data Spectrum Corporation) of 2.5 mm thickness each. The phantom was suspended in the centre of the transaxial FOV and parallel to the scanner axis with a dedicated manufacturer support. Five emission scans of two minutes each were repeated adding one of the aluminium sleeves. Measurements were acquired with the source centred in the FOV and at 10 cm radial offset from the centre of the transaxial FOV.

Two-dimensional sinograms were created using a single slice rebinning for each acquisition. Estimated random counts were subtracted. The five true count rates corrected for decay were plotted in function of the aluminium thickness and fitted with an exponential model. The count rate to an attenuation free condition was extrapolated. The sensitivity values at the centre and at 10 cm radial offset from the centre of the FOV were defined as the count rate attenuation free divided by the activity in the line. The axial sensitivity profile of the system was generated using the data collected for the smallest sleeves at the 0 cm radial offset.

2.4. Spatial resolution

Radial, tangential and axial spatial resolution was measured imaging a point source in air. A glass capillary tube (inner diameter inferior than 1 mm) containing a drop of 18F-FDG with an activity between 1.8 and 3.7 MBq was suspended in air in 10 different positions. In the transverse direction, the source was positioned at 1, 10 and 20 cm from the centre of the plane, while, in the axial direction, it was positioned at the centre and at 3/8th of the axial FOV (6,75 mm). Position accuracy was guaranteed by a support plus an acquisition protocol for Point

Source Centering check provided by the manufacturer. The capillary tube was positioned parallel to the scanner axis for transversal and radial measurements and orthogonal for axial measurements, in order to limit the axial extent of the source to the inner diameter of the capillary (1 mm).

Data were acquired until three million counts were collected. Images were reconstructed using 3D Filter Back Projection with a ramp filter and 1 mm pixel size.

The width of the reconstructed image point spread function in all three directions was evaluated. The maximum of each profile was determined using a parabolic fit; FWHM and FWTM were determined by linear interpolation between adjacent pixels at half or one tenth of the maximum value of the response function in the radial, tangential and axial directions.

2.5. Scatter fraction, count losses and random measurement

A 70 cm polyethylene tube (internal diameter: 3.2 mm) filled with an average activity of 566 MBq (564.4–568 MBq) of 18F-FDG (the manufacturer's suggested activity was between 555 and 629 MBq) was placed parallel to the central axis of a cylindrical polyethylene scatter phantom (NEMA Scatter Phantom Set, Data Spectrum Corporation). The phantom was positioned on the scanner table parallel to the scanner axis, in the centre of the FOV.

Thirty regular emission frames were recorded while the activity in the phantom decayed over several half-lives, until true event losses were less than 1%. The duration of the individual acquisitions was less than one-fourth of the isotope half-life. Each acquisition had to contain a minimum of 500.000 prompt counts. Images were acquired using the manufacturer's protocol for a total time of 16 h. Uncorrected prompt and random sinograms were generated and rebinned using single-slice rebinning. The sinograms were then processed to calculate the scatter fraction as well as the true, random, scatter, noise-equivalent and total count rates for each slice. The Noise Equivalent Count Rate (NECR) for each acquisition was obtained as the sum of all the slices. The NECR curve peak and the maximum true event rate were calculated.

2.6. Accuracy for count losses and random events

Accuracy of correction for dead time losses and random events was measured using the data acquired for the scatter fraction, count losses and random measurements. Reconstruction with scatter, dead time, random and attenuation corrections was performed using the standard whole body algorithm. A centred circular region of interest (18 cm diameter) was defined in each transaxial slice and in each reconstruction; the true count rate in the region was measured. The true count rate in the absence of random events and dead-time losses was estimated by averaging the lowest activity acquisitions (below the NECR peak). The relative count rate error was computed for each slice for each acquisition.

2.7. Image quality

Image quality and noise were tested using the NEMA anthropomorphic thorax phantom (NEMA IEC Body Phantom Set and NEMA Scatter Phantom Set, Data Spectrum Corporation) containing six spheres (internal diameters of 10, 13, 17, 22, 28 and 37 mm), simulating both cold and hot lesions. The four smallest spheres were filled with radioactive water, and the two largest, with cold water. A cylindrical insert filled with low density foam (density of 0.30 g/cm^3) was fixed along the centre of the phantom. Four to 1 Sphere to Background Ratio (SBR) was realized (average SBR = 4.0, range: 3.9 – 4.0), using a solution with an average activity of 52 MBq (50–54 MBq) of 18F-FDG (the manufacturer's suggested activity was 51.8 MBq) and water in the NEMA IEC Body Phantom cavity volume (9900 ml) in order to realize an activity concentration of the background equal to 5.3 kBq/cc. A 70 cm polyethylene tube filled with 100.9–130 MBq of 18F-FDG (the manufacturer's suggested activity was 103.6 MBq) was placed in the polyethylene scatter phantom used for scatter fraction, count losses and random measurements. The phantom was centred in the transverse FOV of the scanner with the centre of the spheres coplanar to the centre of the axial FOV. The scatter phantom was placed behind the Body phantom to simulate activity outside the scanner.

Images were acquired in list-mode with one bed position of 2 min and 31 s. A CT scan was used for attenuation correction. Images were reconstructed according to the manufacturer's "Head&Neck" protocol, suggested for NEMA Image Quality analysis, with the Speed parameter set to High Quality (3 iterations, 33 subsets, 23 cm-TOF kernel), Smooth/sharp set to SmoothB, and the application of PSF with 1 recovery iteration and a 6.0 mm FWHM regularization kernel, 2 mm isotropic voxel.

The percentage hot (H_CRC) and cold (C_CRC) Contrast Recovery Coefficient (CRC), the background variability (BV) and the residual lung error were calculated according to NEMA NU-2 2012 standards.

2.8. Image quality with different reconstruction settings

Image quality in terms of H_CRC, C_CRC and BV was tested on an NEMA IEC Body Phantom Set with an SBR 4 and 8 to 1 (average SBR = 8.3, range: 8.0–8.7).

Both NEMA IEC Body Phantom realizations were reconstructed by changing the available reconstruction parameters, as shown in Table 1. All the possible reconstruction parameter combinations were tested, changing the "Smooth/Sharp" and the "Speed" parameters. Images were also processed with PSF correction, setting one or two iterations and varying the regularization kernel between 5 and 7 mm. C_CRC, H_CRC and BV were calculated according to NEMA NU-2 2012 standards for each image.

Standard reconstruction suggested for whole-body clinical application were Normal Speed and Normal Smooth with 4 mm isotropic voxel.

2.9. Statistical analysis

All the performance measurements were repeated once in each centre, for a total of three different measurements. The mean and the range of each parameter were calculated for each test.

The samples of CRC and BV data coming from the three different PET/CT scanners were tested by means of one way ANOVA ($p < 0.05$) to identify potential differences in data coming from different scanners.

Box plots were used to provide a univariate graphical representation of the dependent variables (H_CRC, BV and C_CRC) with respect to different reconstruction parameters reported in Table 1.

Correlation matrices and *t*-test were used to identify potential correlations between image quality (H_CRC and BV) and reconstruction parameters (sphere diameters (SphereID), SBR, TOF-kernel, number of equivalent iterations (IT-EQ), amplitude of the Gaussian filter (FWHM), PSF iterations (PSF-IT) and PSF Gaussian regularization kernel width (PSF-Reg)).

Only significant predictors were considered and inserted into multiple linear regression methods to derive analytical formulas of the model.

Table 1
Different reconstruction settings used for NEMA IEC Body phantom reconstructions.

Parameter (meaning)	Values
Speed (Number of iterations)	60, 99, 99
Smooth (Amplitude of Gaussian filter, FWHM)	4, 5, 6, 7 mm
TOF kernel	14.1, 18.7 cm
PSF iterations	1, 2
PSF regularization	5, 6, 7 mm

Table 2
NEMA NU2-2012 sensitivity measures for 0 and 10 mm radial offset.

	Radial offset	Average [range] (reference)
Sensitivity [cps/kBq]	0 cm	7.88 [7.58–8.12] (> 7)
	10 cm	7.91 [7.43–8.41] (> 7)

The statistical analysis was performed with the software STATISTICA 6.0 Statsoft Inc, USA.

The image reconstructed with parameters suggested by the manufacturer for clinical application (Normal Smooth and Normal Speed) was used as the reference.

3. Results

3.1. Energy resolution and timing resolution

The estimated average energy resolution is 10.83% (10.06–11.25%), while the timing resolution is 536.2 ps (528.0–546.6).

3.2. Sensitivity

Sensitivity values are reported in Table 2. The mean (range) central and 10 cm offset average sensitivity values are 7.88 and 7.91 cps/kBq, in agreement with Philips declared value of 7 cps/kBq. Slice sensitivity profiles are reported in Fig. 1 for each scanner.

3.3. Spatial resolution

The axial, radial and tangential resolutions for each radius are reported in Table 3, as average and range of the values obtained in the three centers. Reference values provided by the manufacturer are reported in Table 3 in round brackets.

3.4. Scatter fraction, count losses and random measurement

Count rate curves of the three centres measured with the NEMA scatter phantom are reported in Fig. 2. The average maximum NECR was 119.83 (116.39–122.70) kcps at 20.67 (19.21–22.53) kBq/ml, in agreement with the Philips declared value of > 110 kcps at 15 kBq/ml.

The maximum true event rate was 322.62 (321.26 – 325.10) kcps at a concentration of 24.51 (22.53–25.63) kBq/ml in the phantom, in agreement with Philips declared value of > 225 kcps at 25.628 kBq/ml. The scatter fraction was 30.37 (29.24–31.33) at NECR peak, well below the < 35% upper limit declared by the manufacturer.

3.5. Accuracy for count losses and random events

The maximum bias below NECR peak was 12.58% (8.84–18.20%), in agreement with Philips declared upper limit value of 30%.

3.6. Image quality

Results of CRC, BV and lung error for both SBR with the reconstruction parameter suggested by the manufacturer for the image quality test are reported in Table 4. Reference values, relative to 4 to 1 SBR, are provided by the manufacturer only for CRC and BV and are reported in Table 4 in round brackets.

BV and lung error were comparable between the two acquired SBR, while CRC values were higher for 8 to 1 images, as expected. All the CRC and BV values for the 4 to 1 SBR were in agreement with the reference value declared by the manufacturer.

3.7. Comparison with previous scanner model

A detailed comparison between PET performances obtained in this multicentre study and the results of Kolthammer et al. [2] on the previous Ingenuity TF model and of Surti et al. [7] on the Gemini TF model is reported in Table 5. Surti et al. [7] performed the acceptance measures according to the NEMA NU-2 2001 Standards [8], while Kolthammer et al. [2] followed the NEMA NU-2 2007 standards [3]. Comparison of results is possible because the main differences among the three standards is related to the spatial resolution source position.

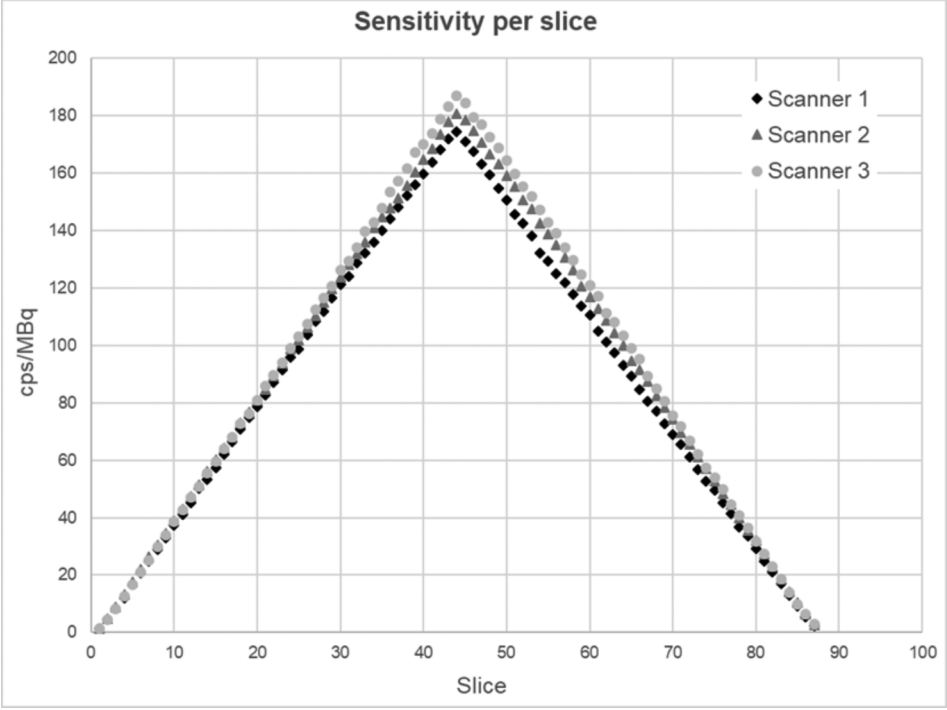

Fig. 1. Slice sensitivity profiles for the three scanners.

Table 3
NEMA NU2-2012 axial, radial and tangential resolutions; FWHM: full width at half maximum, FWTM: full width at tenth maximum.

	Transverse position	FWHM/FWTM	Profile	Average [range] (reference)
Spatial resolution	1 cm	FWHM [mm]	Transversal	4.74 [4.66–4.88] (< 5.1)
			Axial	4.74 [4.71–4.79] (< 5.1)
		FWTM [mm]	Transversal	9.61 [9.50–9.74]
			Axial	9.63 [9.62–9.64]
	10 cm	FWHM [mm]	Radial	5.14 [5.07–5.21] (< 5.5)
			Tangential	4.96 [4.92–5.00] (< 5.5)
			Axial	4.74 [4.69–4.84] (< 5.5)
		FWTM [mm]	Radial	10.25 [10.16–10.31]
			Tangential	9.91 [9.82–9.99]
			Axial	9.65 [9.59 9.75]
	20 cm	FWHM [mm]	Radial	6.11 [6.00–6.25] (< 7.2)
			Tangential	5.34 [5.31–5.36] (< 7.2)
			Axial	5.01 [4.94–5.05] (< 7.2)
		FWTM [mm]	Radial	11.24 [11.12–11.48]
			Tangential	11.26 [11.22–11.33]
			Axial	10.00 [9.83–10.11]

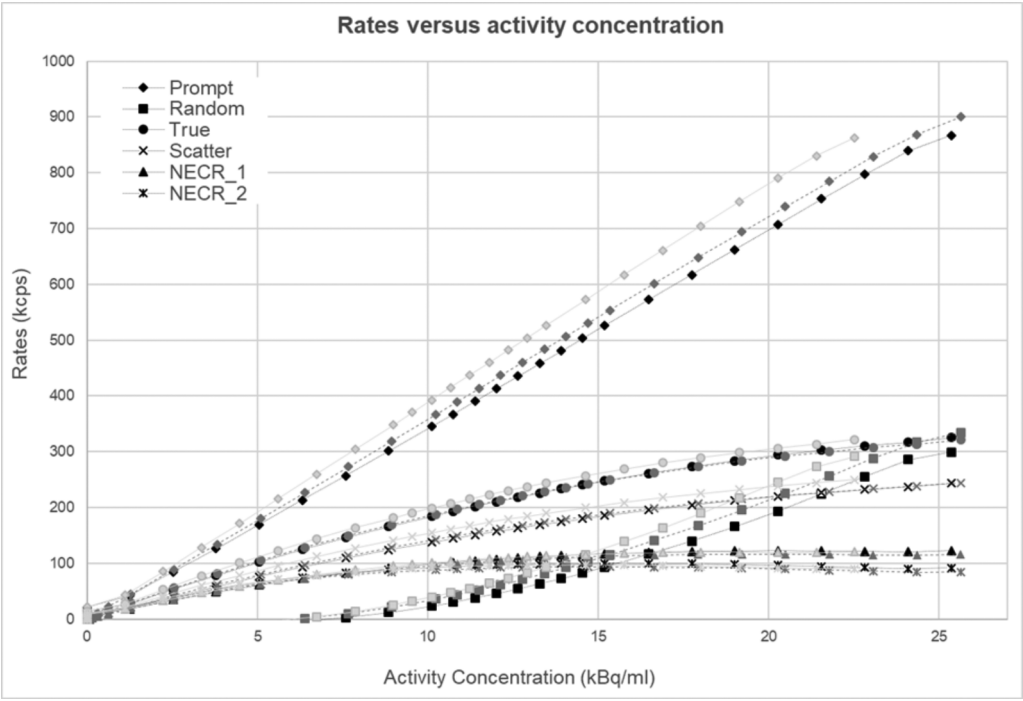

Fig. 2. Count rate curves in function of the activity concentration; black, gray and light gray curves represent scanner of centre 1, 2 and 3, respectively.

3.8. Image quality with different reconstruction settings

The ANOVA test reported no significant differences among PET/CT scanners on CRC ($F = 1.4$; $p = 0.24$) and BV ($F = 2.2$; $p = 0.11$) values, respectively.

The dependence of H_CRC on different reconstruction parameters may be better understood by means of box plot. Fig. 3a and b show the higher impact of PSF on H_CRC: PSF application increases median H_CRC values of +32% and +50% for 1 and 2 iterations, respectively, when compared to median H_CRC obtained with different Speed parameters (Fig. 3a). In a similar way, Fig. 3b shows the increase in H_CRC with PSF iteration 1 (+33%) and 2 (+51%), with respect to different Smooth parameters. Speed and Smooth parameters have no influence on contrast recovery coefficient.

In a similar way, the dependence of BV on PSF-IT, and Smooth parameters, as well as the non dependence on Speed, may be better understood by means of box plot, as shown in Fig. 4a and b, which clearly show the highest impact of PSF (median increase of +27% and +39% for 1 and 2 iterations respectively) and Smooth on BV, and the absence of impact of Speed.

The limited dependence of C-CRC on PSF-IT and Speed parameters is clearly reported by the box plot in Fig. 5.

Correlation matrices and *t*-test showed that only SphereID and PSF-IT had a statistically significant impact on H_CRC, while only SphereID, PSF-IT and FWHM had a statistically significant impact on BV.

Results of the multiple linear regression analysis are reported in Table 6, where the weight (βi) and the regression coefficients (Bi) for each independent variable are reported.

The regression equation that best summarizes the results obtained in a multiple regression model with H_CRC as predicted variable and SphereID, PSF-IT as predictor variables can be written as:

$$H\_CRC = -10.3 + 3.5 * SphereID + 10.2 * PSFIT$$

The multiple R^2 of model fitting equals to 0.93. SphereID is the parameter with the highest weight explaining the model expression ($\beta = 0.84$), followed by PSF-IT ($\beta = 0.41$). SBR, PSFreg, TOF-kernel, FWHM and IT-EQ have no impact on H_CRC.

The regression equation that best summarizes the results obtained in

Table 4
NEMA NU-2 2012 image quality results of the 4 to 1 and 8 to 1 SBR, with the following reconstruction parameters: speed = High Quality, smooth = SmoothB, PSF correction with one iteration and regularization kernel equal to 6 mm, 2 mm isotropic voxel. Ranges were reported in square brackets, reference values in round brackets.

Parameter	SBR:4 Sphere diameter [mm]						SBR:8 Sphere diameter [mm]					
	10	13	17	22	28	37	10	13	17	22	28	37
CRC [%]	39.0 (> 26) [34.0–45.4]	56.4 (> 40) [49.9–61.8]	70.1 (> 50) [63.7–75.8]	77.2 (> 60) [72.6–82.8]	73.1 (> 68) [71.3–74.2]	77.2 (> 70) [75.4–78.2]	54.2 [48.3–57.8]	71.7 [64.3–78.9]	79.4 [69.3–89.9]	85.4 [77.1–99.0]	74.5 [72.2–76.4]	80.5 [77.1–83.9]
BV [%]	8.5 (< 11) [7.4–10.2]	7.0 (< 9) [6.3–8.3]	5.4 (< 8) [5.02–6.22]	4.3 (< 8) [4.0–4.8]	3.6 (< 7) [3.3–3.9]	3.02 (< 7) [2.9–3.2]	9.1 [8.0–10.7]	7.6 [6.8–9.0]	5.9 [4.9–7.0]	4.6 [3.5–5.2]	3.9 [2.7–4.8]	3.4 [2.3–4.7]
Lung Error [%]	14.7 [14.5–15.1]						14.0 [13.4–15.0]					

a multiple regression model with BV as predicted variable and SphereID, PSF-IT and FWHM as predictor variables can be written as:

$$BV = 8.1 - 0.1 * SphereID + 0.7 * PSFIT - 0.3 * FWHM$$

The multiple R^2 of model fitting equals 0.86. SphereID is the parameter with the highest weight explaining the model expression ($\beta = 0.69$), followed by PSF-IT ($\beta = 0.34$) and FWHM ($\beta = 0.23$). TOF-kernel, IT-EQ and PSFreg have no effect on BV.

Representative axial views of the NEMA IEC Body Phantom with different reconstruction settings for the 8 to 1 SBR are reported in Fig. 6.

4. Discussion

The Ingenuity TF PET/CT RoHS belongs to the latest generation of the non-digital PET/CT scanners. It incorporates a TOF-capable PET scanner with a PIXELAR detector design. The results of the performance evaluation according to the NEMA NU-2 2012 standards in this multicentre study show a transaxial spatial resolution (1 cm from the centre of FOV) of 4.7 mm and an absolute system sensitivity of 7.9 cps/kBq in the scanner centre. All the results of NEMA tests were below the limit declared by the manufacturer. The multicentre characteristics of this work guarantees robustness to the results obtained.

Table 5 reported a detailed comparison between PET performances obtained in this multicentre study and the results of Kolthammer et al. [2] on the previous Ingenuity TF model and of Surti et al. [7] on the Gemini TF model.

PET detector design is comparable among these different models: most characteristics of the upgraded Ingenuity TF are equivalent to the previous model and to the Gemini TF. These include type and crystal dimension, TOF capability, number of modules and the PIXELAR technology. The main innovative element of the upgraded version is the new design of the electronics, realized to be compliant to the RoHS European council directive 2002/95/CE. Therefore, the upgraded scanner reaches better performance with a 3.8 ns coincidence window for the 576 mm FOV, which is shorter with respect to the previous model (4.5 ns) [2] and to Gemini TF (6.0 ns) [7].

The absolute sensitivity in the FOV centre measured in this work (7.9 cps/kBq) is superior with respect to the previous Ingenuity model (7.4 cps/kBq) [2] and Gemini TF (6.6 kBq/ml) [7]. This means that the reduced coincidence window does not decrease the true system sensitivity. The measured spatial resolution is comparable to the previous results because the crystal dimension does not change between Gemini TF and Ingenuity TF. The 20 mm offset measurement introduced by the 2012 NEMA standards demonstrates a small degradation in resolution moving away from the centre of the FOV.

A good average energy resolution allows a narrow energy window (440 – 715 keV) that leads to a reduction in the system scatter fraction with respect to the previous model. Additionally, the system scatter fraction remains stable at different activity concentration levels.

As a result of the innovative high quality electronics, the Noise Equivalent Count Rates obtained in this multicentric study show a peak position at higher scanner rates (20.67 kBq/ml) with respect to Gemini TF (17.4 kBq/ml). The higher count rate performance is particularly important for cardiac imaging or dynamic studies.

The results obtained for the Ingenuity TF are comparable to other commercial scanners with similar system geometry, type of scintillators (LYSO or LSO), TOF capability and crystal dimensions [9,10,11].

In this study, a detailed analysis of the influence of reconstruction parameters and application of PSF correction on CRC and BV values derived from IEC phantom measurements was performed. Reconstruction settings were selected in order to reproduce the best possible typical whole body adult protocol for oncological patients (4 mm voxel size).

The most important result is that application of PSF correction with 1 or 2 iterations always led to CRC values lower than 100%, regardless

Table 5
Comparison of PET performance between the results obtained in this study, on the previous model of Ingenuity TF [2] and on Gemini TF [7]. Measures by Surti et al. [7] were executed according to NEMA NU-2 2001 Standards [8], while Kolthammer et al. [2] followed NEMA NU-2 2007 Standards [3]. n.e.: not executed; n.r.: not reported (values of Surti et al. were not reported because CRC were obtained with a different reconstruction algorithm); *: CRC values obtained with an acquisition of 10 min and reconstruction with body detail protocol with PSF correction.

Parameters			Ingenuity TF – RoHS	Ingenuity TF	Gemini TF
Coincidence window [ns]			3.8	4.5	6
Timing resolution [ps]			536.2 [528.0–546.6]	502	585
Energy resolution [%]			10.83 [10.06–11.25]	11.1	11.5
Sensitivity [cps/kBq]	R0		7.88 [7.58–8.12]	7.39	6.6
	R10		7.91 [7.43–8.41]	7.28	
Spatial resolution FWHM [mm]	1 cm	Transversal	4.74 [4.66–4.88]	4.84 ± 0.13	4.8
		Axial	4.74 [4.71–4.79]	4.73 ± 0.07	4.8
	10 cm	Radial	5.14 [5.07–5.21]	5.25 ± 0.16	5.2
		Tangential	4.96 [4.92–5.00]	5.01 ± 0.07	5.2
		Axial	4.74 [4.69–4.84]	5.23 ± 0.37	4.8
	20 cm	Radial	6.11 [6.00–6.25]	n.e.	n.e.
		Tangential	5.34 [5.31–5.36]	n.e.	n.e.
		Axial	5.01 [4.94–5.05]	n.e.	n.e.
NECR peak [kcps, kBq/ml]			119.83 [116.39–122.70], 20.67 [19.21–22.53]	124.1, 20.3	125.0, 17.4
Maximum true event rate [kcps, kBq/ml]			322.62 [321.26–325.10], 24.51 [22.53–25.63]	364.5, 35.0	274.0, 17.4
SF @ NECR peak [%]			30.37 [29.24–31.33]	36.7	27
Image Quality		10 mm sphere	39.0 [34.0–45.4]	39*	n.r.
H_CRC [%]		13 mm sphere	56.4 [49.86–61.76]	73*	n.r.
		17 mm sphere	70.1 [63.71–75.78]	74*	n.r.
		22 mm sphere	77.2 [72.6–82.8]	80*	n.r.

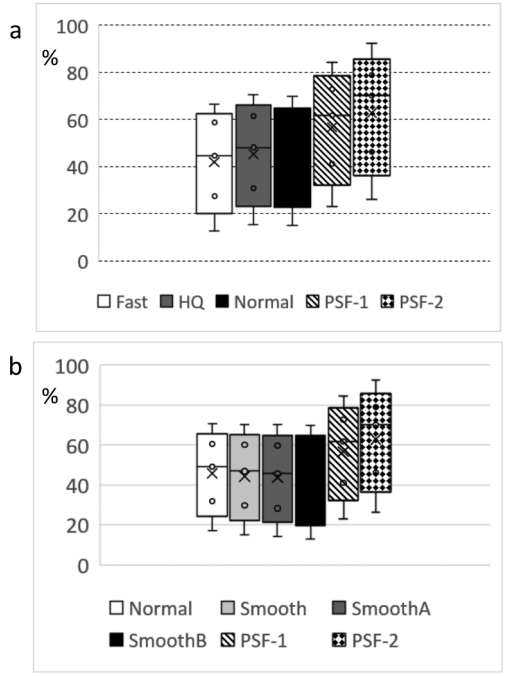

Fig. 3. Boxplot of H_CRC varying speed (a) and smooth (b) parameters. H_CRC values were averaged over all sphere diameters and reconstruction parameters reported in Table 1, except for speed (a) or smooth (b) parameters.

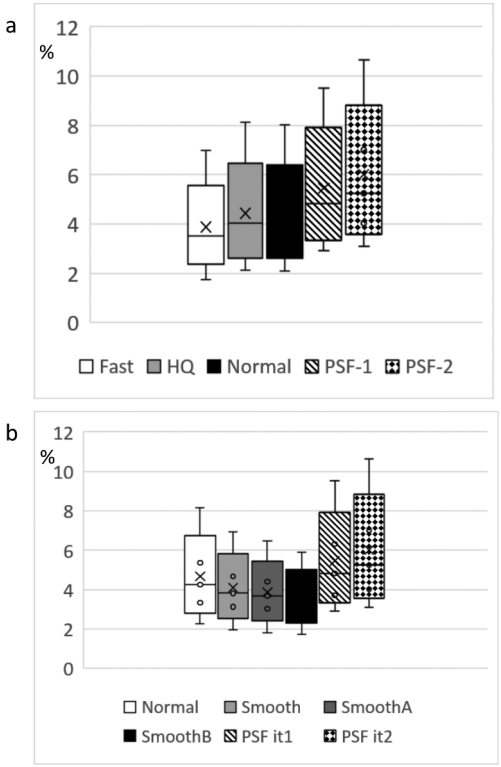

Fig. 4. Boxplot of BV varying the speed (a) and smooth (b). BV values were averaged over all the sphere diameters and the reconstruction parameters reported in Table 1, except for speed (a) or smooth (b).

of the reconstruction parameters applied, meaning that the activity concentration recovered in the spheres in the range 10–22 mm is never overestimated. It's not guaranteed that no overcorrection will be the case also for narrower post-reconstruction filters.

This is an important issue, as the literature reports cases of overestimation in recovery coefficients [12,13] or SUV values [14] and a non-monotonical increasing trend in recovery coefficients with sphere dimension [13] when resolution modelling is applied, especially in the range 13–22 mm.

Neither the edge nor Gibbs artifacts [15] were observed in any of the IEC phantom images reconstructed in the range of the reconstruction settings evaluated in this study. This may be related to the presence of the noise-regularization parameter (PSF-reg) in the Ingenuity TF resolution recovery algorithm that not only controls the noise but also has an impact on the recovery of the activity [6,16]. The regularization values used in this work (5–7 mm) were close to the system spatial resolution, as suggested by the manufacturer. When the regularization values are much greater than the actual scanner resolution, PSF correction is likely to create edge artefacts

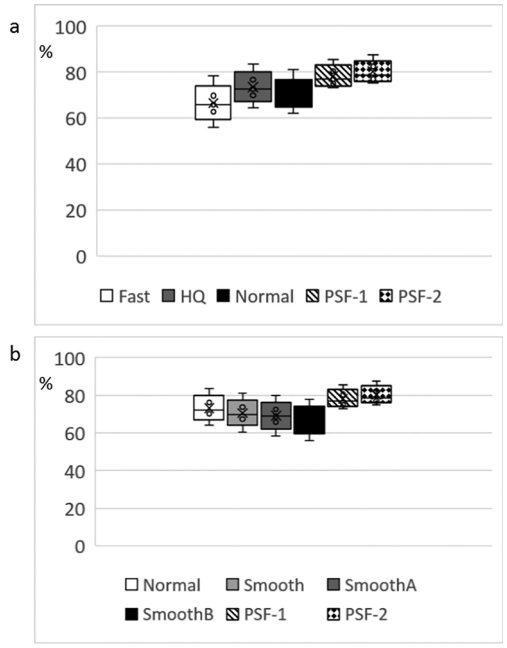

Fig. 5. Boxplot of C_CRC varying the speed (a) and smooth (b). C_CRC values were averaged over all the sphere diameters and the reconstruction parameters reported in Table 1, except for speed (a) or smooth (b).

Table 6
Results of the multiple linear regression analysis including PSF correction. For each independent variable, the weight of the variable in the model, the coefficient in the analytic expression (with standard deviation) and p-level were reported.

Parameter	Independent Variable	*β*	*B*	*p-level*
H_CRC	SphereID	0.84	3.5 ± 0.1	0.00000
	PSF-IT	0.41	10.2 ± 0.4	0.00000
BV	SphereID	−0.69	−0.1 ± 0.0	0.00000
	PSF-IT	0.29	0.6 ± 0.1	0.00000
	FWHM	−0.22	−0.3 ± 0.0	0.00000

and overestimation of the activity.

The effect of PSF correction on the CRC of cold spheres was of limited value for two reasons. First, the aim of PSF correction is to increase the recovery of the activity in a target: since the target is cold, the correction is less effective. Second, only the two biggest spheres (28–37 mm) in the IEC phantom were filled with non-radioactive water, accordingly to NEMA 2012 indications: thus, it is not surprising that CRC increase is only marginal (+12%) when PSF is applied with respect to Normal, Fast and HQ speed reconstruction images as the dimension of these spheres is up to 6 fold the spatial resolution of this PET scanner. Similar results are reported by Reynés-Llompart [17] for the Discovery IQ PET scanner, and by Bettinardi et al. for the Discovery 690 [18] and for the Biograph mCT [19].

A multiple linear regression analysis was performed to predict the influence of different reconstruction parameters and PSF correction on H_CRC and BV, calculated for NEMA Image Quality phantom.

As far as H_CRC is concerned, the multiple $R^2 = 0.93$ obtained indicates that the model adopted to explain H_CRC variability is good. H_CRC is strongly dependent on sphere dimension ($\beta = 0.84$), as it may obviously be argued, and, for a fixed sphere dimension, on the application of PSF correction which is the second parameter that impacts H_CRC in order of relevance ($\beta = 0.41$). The sphere-to background ratio of a lesion has no impact on H_CRC and the identical conclusion applies to the number of equivalent iterations, amplitude of Gaussian filter, TOF kernel and the regularization parameter of PSF.

These results indicate that for a given lesion, the unique way to increase its H_CRC is to apply PSF correction, as changing the number of equivalent iterations, the TOF kernel or the amplitude of the Gaussian filter have no effect on H_CRC. This can be clearly understood by looking at the box plot of Fig. 3a, which shows an overall median increase of about 32% and 50% in H_CRC of all spheres of both SBR obtained by applying PSF with 1 and 2 iterations, respectively, when compared to the corresponding increase obtained by changing the Speed parameter. In a similar way, Fig. 3b shows the absence of effect of Smooth parameter on H_CRC, as median H_CRC values obtained with application of PSF. An increase was observed: on average, about 33% and 51% for 1 and 2 iterations, respectively, when compared with different Smooth parameters, where box plots are obtained by averaging H_CRC values on all parameters, with the exception of Smooth and PSF.

The relevance of PSF correction in increasing H_CRC is not surprising, since PSF correction was intentionally devised to improve the

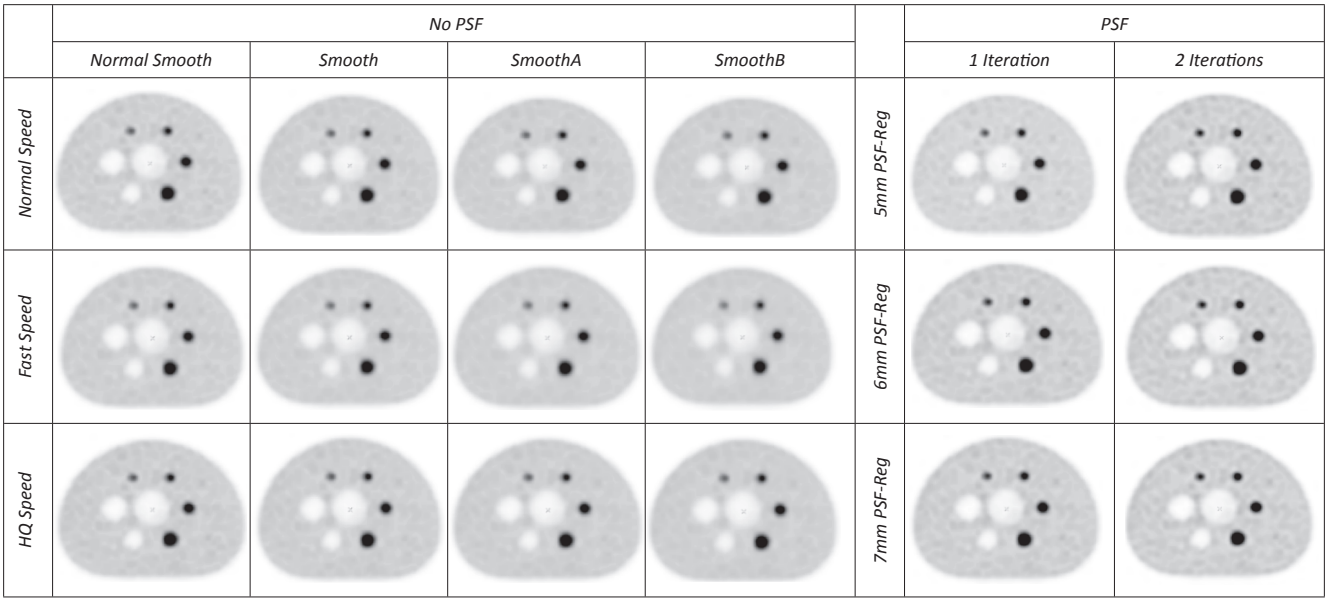

Fig. 6. Axial view of image quality phantom with different reconstruction parameters, SBR equal to 8 to 1.

spatial resolution and image quality of PET images.

The non-dependence of H_CRC on the number of equivalent iterations and amplitude of the gaussian filter is in agreement with the qualitative analysis that can be done by inspecting Fig. 6.

The multiple linear regression equation obtained for BV (R^2 = 0.86) shows that this parameter depends on sphere dimension (β = 0.69), PSF iteration (β = 0.34), amplitude of Gaussian filter (β = 0.23), in order of decreasing relevance. The application of PSF increases median BV by 27% (1 iteration) and 39% (2 iterations) with respect to corresponding median values obtained without PSF application. Its weight is only slightly superior to that of the amplitude of the Gaussian filter, meaning that the user can try to reduce the BV when applying the PSF correction, by acting only on a smoothing filter [13], as the number of equivalent iterations has a limited influence on BV, as box plots in Fig. 4a and 4b show.

Finally, this multicentre study provides information on the variability of image quality parameters, due to both phantom preparation, positioning and acquisition. Mansor et al [20] evaluated the recovery coefficient's variability using the NEMA image quality phantom acquired on the Ingenuity PET/CT scanner and on the Biograph mCT 40, by introducing random repositioning of the phantom and varying the image reconstruction parameters. The authors observed that repositioning of the phantom increased variability of recovery coefficient data compared with the stationary phantom data especially for the Philips Ingenuity PET/CT scanner and when image are reconstructed with PSF correction. The variability of our H_CRC data (Table 5) is larger than that obtained by Mansor and colleagues, and this result can be easily explained by considering that phantom preparation may represent the major source of variability, rather than the simple repositioning operation.

Some limitations of the study need to be acknowledged.

First, the results on H_CRC found in the present study strictly apply to the range of the explored lesion dimensions and SBR and cannot be extrapolated outside these ranges. Actually, it would be interesting to know whether the application of PSF correction is still monotonical for lesion dimensions smaller than 10 mm and greater than 22 mm, and for all clinical SBR values, to guarantee the accuracy in image quantitation.

Second, the BV as defined by NEMA Standards is the percent variation of the signal in the background, but it cannot be assumed as a measure of noise [21]. Rather, noise is quantified using different metrics, especially when in presence of a resolution modelling algorithm as reported by Rahmim [22]. But this analysis was beyond the aim of this study.

Third, the contrast-to-noise ratio analysis of hot target was not afforded in this study: it would, however, add important information to lesion detectability in whole body clinical studies, which is the ultimate task of the nuclear medicine physician.

5. Conclusions

The new Ingenuity TF model with PIXELAR detector design shows physical performance similar to other scanners of the latest generation for all the standard NEMA NU-2 2012 measurements. It reveals better or comparable performances with respect to the previous Ingenuity TF model and Gemini TF. The PSF reconstruction algorithms allow contrast recovery coefficient improvements for a better quantitative performance. Background variability increase caused by PSF correction could be balanced by additional Gaussian filtration, obtaining high quality images while keeping the noise at an acceptable level.

Declaration of Competing Interest

The authors declare that they have no known competing financial interests or personal relationships that could have appeared to influence the work reported in this paper.

Acknowledgements

The authors would like to thank Dr. Dmitri Sutov for his support during the training period in the Veneto Institute of Oncology IOV-IRCCS.

References

[1] NEMA Standards Publication NU2-2012. Performance measurements of positron emission tomographs. Rosslyn: National Electrical Manufacturers Association; 2013.
[2] Kolthammer JA, Su KH, Grover A, Narayanan M, Jordan DW, Muzic RF. Performance evaluation of the Ingenuity TF PET/CT scanner with a focus on high count-rate conditions. Phys Med Biol 2014;59(14):3843–59. https://doi.org/10.1088/0031-9155/59/14/3843.
[3] NEMA Standards Publication NU2-2007. Performance measurements of positron emission tomographs. Rosslyn: National Electrical Manufacturers Association; 2008.
[4] Devriese J, Beels L, Maes A, Van de Wiele C, Pottel H. Impact of PET reconstruction protocols on quantification of lesions that fulfil the PERCIST lesion inclusion criteria. EJNMMI Phys 2018;5(1):35. https://doi.org/10.1186/s40658-018-0235-6.
[5] Philips NM Clinical Science, Enhanced lesion detectability and accurate quantitative imaging, White Paper, Philips Healthcare, USA.
[6] Philips NM Clinical Science, Resolution recovery in the Ingenuity TF PET/CT, White Paper, Philips Healthcare, USA.
[7] Surti S, Kuhn A, Werner ME, Perkins AE, Kolthammer J, Karp JS. Performance of Philips Gemini TF PET/CT scanner with special consideration for its time-of-flight imaging capabilities. J Nucl Med 2007;48(3):471–80.
[8] NEMA Standards Publication NU2-2001. Performance measurements of positron emission tomographs. Rosslyn: National Electrical Manufacturers Association; 2002.
[9] Slomka PJ, Pan T, Germano G. Recent advances and future progress in PET instrumentation. Semin Nucl Med 2016;46(1):5–19. https://doi.org/10.1053/j.semnuclmed.2015.09.006.
[10] Van der Vos CS, Koopman D, Rijnsdorp S, et al. Quantification, improvement, and harmonization of small lesion detection with state-of-the-artPET. Eur J Nucl Med Mol Imaging 2017;44(Suppl. 1):4–16. https://doi.org/10.1007/s00259-017-3727-z.
[11] Surti S, Karp JS. Advances in time-of-flight PET. Phys Med 2016;32(1):12–22. https://doi.org/10.1016/j.ejmp.2015.12.007.
[12] Knäusl B, Hirtl A, Dobrozemsky GPET, et al. based volume segmentation with emphasis on the iterative TrueX algorithm. Z Med Phys 2012;22(1):29–39. https://doi.org/10.1016/j.zemedi.2010.12.003.
[13] Munk OL, Tolbod LP, Hansen SB, Bogsrud TV. Point-spread function reconstructed PET images of sub-centimeter lesions are not quantitative. EJNMMI Phys 2017;4(1):5. https://doi.org/10.1186/s40658-016-0169-9.
[14] Matheoud R, Ferrando O, Valzano S, et al. Performance comparison of two resolution modeling PET reconstruction algorithms in terms of physical figures of merit used in quantitative imaging. Phys Med 2015;31(5):468–75. https://doi.org/10.1016/j.ejmp.2015.04.011.
[15] Snyder DL, Miller MI, Thomas Jr LJ, Politte DG. Noise and edge artifacts in maximum-likelihood reconstructions for emission tomography. IEEE Trans Med Imaging 1987;6(3):228–38.
[16] Yamaguchi S, Wagatsuma K, Miwa K, Ishii K, Inoue K, Fukushi M. Bayesian penalized-likelihood reconstruction algorithm suppresses edge artifacts in PET reconstruction based on point-spread-function. Phys Med 2018;47:73–9. https://doi.org/10.1016/j.ejmp.2018.02.013.
[17] Reynés-Llompart G, Gámez-Cenzano C, Romero-Zayas I, Rodríguez-Bel L, Vercher-Conejero JL, Martí-Climent JM. Performance characteristics of the whole-body discovery IQ PET/CT system. J Nucl Med 2017;58(7):1155–61. https://doi.org/10.2967/jnumed.116.185561.
[18] Bettinardi V, Presotto L, Rapisarda E, Picchio M, Gianolli L, Gilardi MC. Physical performance of the new hybrid PET/CT Discovery-690. Med Phys 2011;38(10):5394–411. https://doi.org/10.1118/1.3635220.
[19] Martí-Climent JM, Prieto E, Domínguez-Prado I, et al. Contribution of time of flight and point spread function modeling to the performance characteristics of the PET/CT Biograph mCT scanner. Rev Esp Med Nucl Imagen Mol 2013;32(1):13–21. https://doi.org/10.1016/j.remn.2012.07.001.
[20] Mansor S, Pfaehler E, Heijtel D, Lodge MA, Boellaard R, Yaqub M. Impact of PET/CT system, reconstruction protocol, data analysis method, and repositioning on PET/CT precision: an experimental evaluation using an oncology and brain phantom. Med Phys 2017;44(12):6413–24. https://doi.org/10.1002/mp.12623.
[21] Brambilla M, Matheoud R, Secco C, Sacchetti G, Comi S, Rudoni M, et al. Impact of target-to-background ratio, target size, emission scan duration, and activity on physical figures of merit for a 3D LSO-based whole body PET/CT scanner. Med Phys 2007;34(10):3854–65.
[22] Rahmim A, Tang J. Noise propagation in resolution modeled PET imaging and its impact on detectability. Phys Med Biol 2013;58(19):6945–68. https://doi.org/10.1088/0031-9155/58/19/6945.